Check for updates

Research Article Volume 13, Issue 3, September 2022, pp. 469-486 International Journal of **Protective Structures**

International Journal of Protective Structures
1–18
© The Author(s) 2021
Article reuse guidelines:
sagepub.com/journals-permissions
DOI: 10.1177/20414196211052062
journals.sagepub.com/home/prs
SAGE

Blast mitigation using polymeric 3D printed auxetic re-entrant honeycomb structures: A preliminary study

Richard Critchley[1,2], Rachael Hazael[2], Kamran Bhatti[3], David Wood[3], Alan Peare[3], Stephen Johnson[2] and Tracey Temple[4]

Abstract

Protection of critical infrastructure in an urban environment is a challenging task, specifically against the vehicle bourne improvised explosive device threat. To design infrastructure to withstand this evolving threat, novel solutions and advanced materials need to be developed. One such material of interest are auxetics. This study experimentally analysed the mitigation of blast response of auxetic re-entrant honeycomb structures, with geometries varying between −ve 30° and +ve 30° using additive manufacturing (3D printing) techniques and non-explosive loading via shock tube. Re-entrant auxetic structures (−ve 15°) exhibited repeatable blast mitigation of 23% and reduced the transmitted pressure and impulse of the blast wave. Further highlighting their potential application as a protective measure to enhance a structures blast survivability.

Keywords

Negative Poisson's ratio, additive manufacturing, blast mitigation, auxetic, shock tube, blast, 3D printing

Introduction

Over the last 40 years improvised explosive events have become a prevalent threat with approximately 88,600 (49%) bombing and explosion incidents occurring between 1971 and 2017 (Draganić et al., 2019). In recent years, vehicle-borne improvised explosive devices have been recognised as a serious threat due to devastating effects on critical infrastructure due to parameters such as large payloads, mobility and concealability (Chen et al., 2015; Hu et al., 2011).

[1]Western New England University, Cranfield, UK
[2]Cranfield University, Cranfield Forensic Institute, Shrivenham, UK
[3]Cranfield University, Centre for Defence Engineering, Shrivenham, UK
[4]Cranfield University, Centre for Defence Chemistry, Shrivenham, UK

Corresponding author:
Richard Critchley, Cranfield University, Cranfield Forensic Institute, Shrivenham, SN6 8LA, UK.
Email: r.critchley@cranfield.ac.uk

© The Authors. Published by SAGE. This is the Author Accepted Manuscript issued with:
Creative Commons Attribution Non-Commercial License (CC:BY:NC 4.0).
The final published version (version of record) is available online at DOI:10.1177/20414196211052062. Please refer to any applicable publisher terms of use.

To counter such threats, the overarching design objective is the protection of structures to ensure minimum casualties and damage. To increase the protection of important infrastructure from blast and debris effects, an assortment of engineering measures can be instigated including; blast-resistant walls, strengthening key components of the structure and providing sufficient standoff (Cormie et al., 2009). Unfortunately, in an urban environment, where terrorism-based events often occur; protection measures are difficult to incorporate, for example, existing infrastructure, high cost and limited space to employ standoff. In an urban environment, the dispersion of the blast wave is a complex event where loading profiles can become amplified to levels exceeding a structures ability to resist such pressures due to channelling effects (Smith et al., 2001).

One such method of providing structural protection against blast loading is the application in the form of sacrificial cladding (Ding et al., 2016). Typically, sacrificial cladding comprises of a cover plate and a crushable cellular material (such as metallic foams), where the plate function is to increase flexure capacity while the core acts as an energy absorber (Ding et al., 2016). Through this synergy and suitable design, under blast loading, massive amounts of energy can be absorbed. To date there has been numerous studies on the design and performance of sacrificial cladding (Andami and Toopchi-Nezhad, 2020; Guruprasad and Mukherjee, 2000a, 2000b; Ma and Ye, 2007a, 2007b; Shirbhate and Goel, 2021), especially metallic foams (Dannemann and Lankford, 2000; Hanssen et al., 2002, 2006; Mukai et al., 1999; Sadot et al., 2005; Shahbeyk et al., 2007; Shim and Yun, 2010; Shim et al., 2012). Metallic foams are typically used due to their low cost, ease of manufacture and procurement, however they are characteristically single use and have been shown to enhance loading once the foam has fully compressed. Therefore, there is a need to utilise novel materials such as auxetics, which have gained popularity within the research community due to their enhanced mechanical properties (including shear resistance (Choi and Lakes, 1991; Evans and Alderson, 2000; Lakes, 1991, 1993; Scarpa and Tomlin, 2000), hardness (Alderson, 1999; Chan and Evans, 1997a; Choi and Lakes, 1991; Evans and Alderson, 2000; Friis et al., 1988; Lakes, 1992; Lakes and Elms, 1993; Scarpa et al., 2002; Smith et al., 1999), toughness (Bezazi and Scarpa, 2007, 2009; Chan and Evans, 1997a; Choi and Lakes, 1991; Evans and Alderson, 2000; Lakes, 1991), stiffness (Bezazi and Scarpa, 2009; Scarpa et al., 2005) and acoustic properties and (Choi and Lakes, 1991; Lakes, 1991, 1992; Scarpa and Smith, 2004; Scarpa et al., 2004)) their negative Poisson's ratio.

While there is an extensive literature base on auxetic foams (Chan and Evans, 1997a, 1997b, 1999a, 1999b; Chen and Lakes, 1995; Choi and Lakes, 1995a, 1995b; Critchley et al., 2013a, 2013b; Evans et al., 1994; Friis et al., 1988; Lakes, 1987; Lakes and Elms, 1993; Lee and Lakes, 1997; Lisiecki et al., 2014; Liu and Hu, 2010), there remains a paucity of research on their applications for blast mitigation (Attard et al., 2020; Gao et al., 2019; Imbalzano et al., 2018; Lan et al., 2019, 2020; Novak et al., 2019; Qi et al., 2017; Remennikov et al., 2019; Wang et al., 2018). To date the majority of studies conducted are computationally based (Grujicic et al., 2013; Imbalzano et al., 2018; Jin et al., 2016; Qi et al., 2013; Xue and Hutchinson, 2004) due to the complex, dangerous and very expensive nature of these physical tests (Novak et al., 2019), although some notable experimental manuscripts are available (Li et al., 2014; Neuberger et al., 2007a, 2007b). Interestingly, the majority of these studies utilise explosive charges of varying geometries located within the near-field of the target, resulting in non-planar loading and localised deformation.

Another reason for the limited literature for blast mitigation is due to the difficulties in generating repeatable auxetic foams using tradition manufacturing methods (Gaspar, 2010). While 3D printing offers a path to address these issues due to its ability to manufacture almost any design with a high repeatability, scalability remains a barrier to commercial adaption. Nonetheless, there have been various studies undertaken using reduced scale auxetic structure of various cell configurations including missing rib cut, re-entrant, arrowhead and star under static and dynamic loading

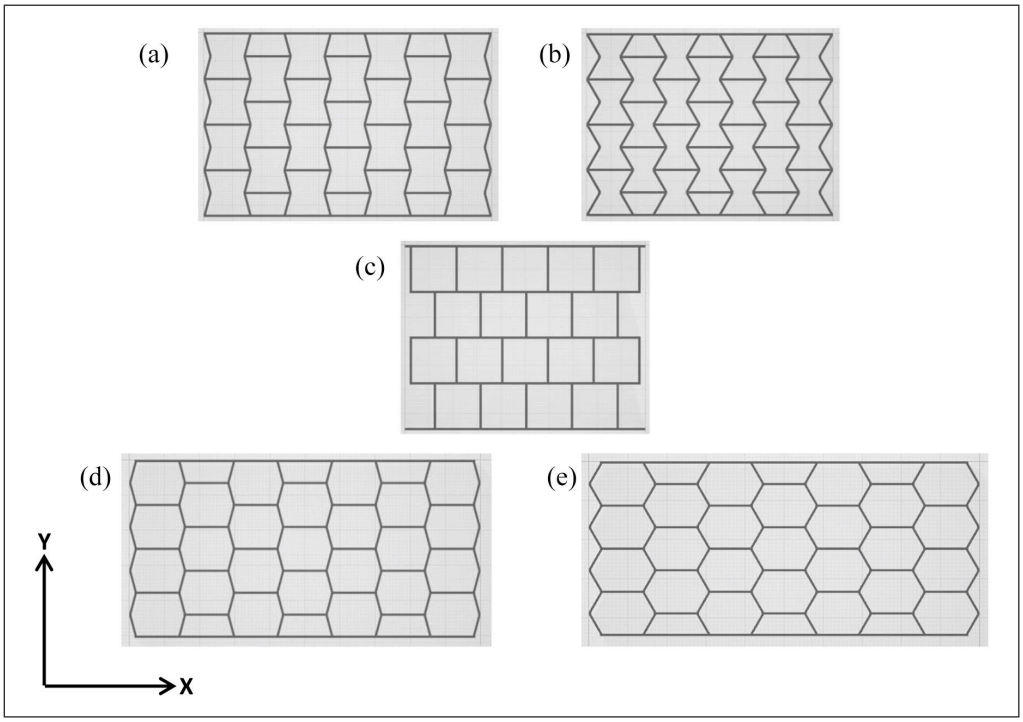


Figure 1. Cellular view of 3D printed structures comprising of: (a) –ve 15° re-entrant cells, (b) –ve 30° re-entrant cells, (c) 0° rectangle cells, (d) +ve 15° honeycomb cells and (e) +ve 30° honeycomb cells. All samples were loaded in the negative *Y*-Axis.

(Dziewit et al., 2017; Habib et al., 2017, 2018; Jiang and Li, 2018; Remennikov et al., 2019), while issues such as scalability are now starting to become overcome by utilising panel sized auxetic structures (Arifurrahman et al., 2020; Kalubadanage et al., 2020).

The approach of this experimental study is to computationally design and 3D print several auxetic re-entrant honeycomb structures of varying pore geometry and to experimentally assess their blast response and behaviour using non-explosive testing.

Materials and methods

Sample preparation

Five structures were computationally designed using Solidworks 2018 64bit (3D computer-aided design software) and are detailed in Figure 1. Each structure comprised of a repeating cell structure. For a given design, the cells had an internal angle of either −30°, −15°, 0°, +15° or +30°. Each cell had a fixed height of 10 mm, a depth of 50 mm and an individual wall thickness of 0.5 mm which when intersected with another cell formed a wall thickness of 1mm. To provide a flat interface at the top and bottom of the structure, base plates were added of dimensions 0.5 mm × 50 mm × 50 mm. Cell details are provided in Figure 2.

Figure 1 illustrates the cellular and complete model view, respectively of all designs fabricated for experimentation. The purpose of keeping these structured dimensions was to design a model as

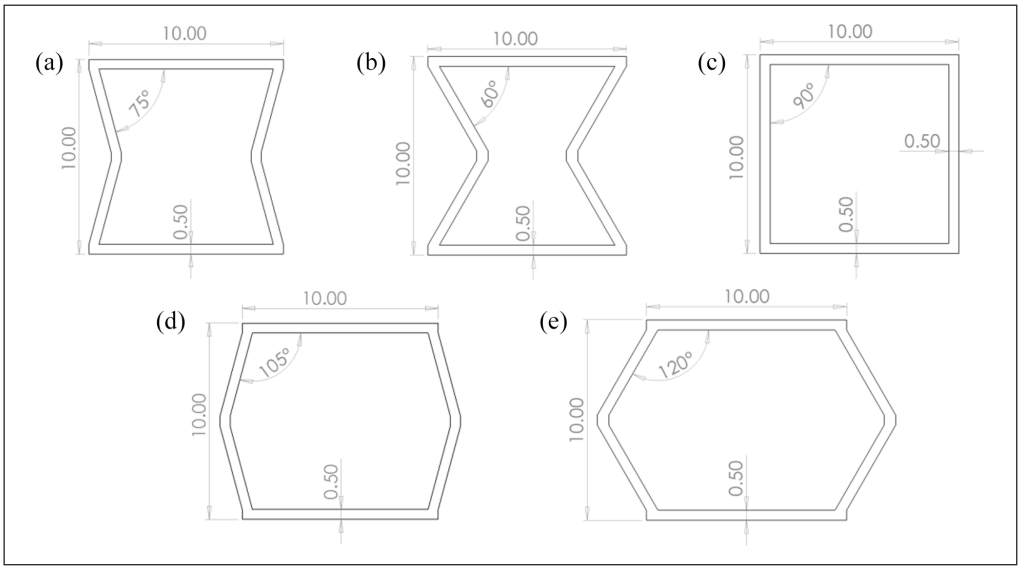


Figure 2. Individual cell dimensions for: (a) –ve 15° re-entrant cells, (b) –ve 30° re-entrant cells, (c) 0° rectangle cells, (d) +ve 15° honeycomb cells and (e) +ve 30° honeycomb cells.

Table 1. Sample dimensions as measured from Solidworks 2018 64bit (3D computer-aided design software) models.

Structure description	Number of tests	Structure dimensions (mm)			Mass (g)	Relative density
		Length	Width	Height		
Baseline (no sample)	4	–	–	–	–	–
−ve 30° re-entrant	4	51.8	50	38.5	19.85	0.16
−ve 15° re-entrant	4	60.06	50	38.5	18.73	0.13
0° rectangle	4	48	50	38.5	18.1	0.16
+ve 15° salient honeycomb	4	81.53	50	38.5	20.13	0.11
+ve 30 salient honeycomb	4	91.02	50	38.5	21.63	0.10

near to rectangle as possible due to the varying length of base-plate in each design. This variation is due to the different angles of structures which are responsible for deciding the overall length of the structured cellular model. Furthermore, with the change in length, the mass of each design also varied between 18.1 and 21.6 g. Table 1 shows the overall dimensions and mass of sample auxetic structures.

For each re-entrant honeycomb design, four samples were fabricated using a fused deposition modelling (FDM) Utimaker three-extended 3D printer using the composite polymeric material thermoplastic polyurethane TPU-95A. TPU-95A was used due to is high levels of elastic deformation required for the cellular structure (Farrell et al., 2020). The material properties of the TPU-95A are documented in (Ultimaker, 2018), with key material parameter detailed in Table 2. All samples were printed along the same orientation to avoid the influence of layer orientation towards the mechanical properties of the material with a layer height of 0.2 mm.[1]

Table 2. Material properties of TPU-95A (Ultimaker, 2018).

Young's modulus	26 MPa
Yield stress	8.6 MPa
Failure stress	39 MPa
Flexural strength	4.3 MPa
Flexural modulus	78.7 MPa
Density	1220 kg m^{-3}
Working humidity	$<$50%

Shock tube testing

A compressed air driven shock tube was used to simulate blast loading in a controlled environment by generating repeatable pressure profiles which resemble high explosive blast waves (Andreotti et al., 2015; Aune et al., 2016; Cormie et al., 2009; Gaskell, 2011). The shock tube located at Cranfield University, Shrivenham, has 600 mm external diameter and 563 mm internal diameter (Figure 3). The tube is rested on supports at 1150 mm above the floor and has 4550 mm length with 500 mm driver section, 50 mm intermediate chamber and 4000 mm driven section.

The shock tube is linked with an external air compressor to facilitate charging of compressed air in the driver section, which is isolated from the driven section through diaphragms. Diaphragms were cut and secured between rubber gaskets with the help of double-sided tape and loaded in the intermediate chamber to ensure an airtight seal between driver and driven section. The pressurised air is charged in the driver section to predetermined limits, whereas the pressure in the driven section is at an ambient level, being open to the atmosphere. Once the pressure inside the driver section exceeds the mechanical strength of the diaphragm, it ruptures and the compressed air from the driver section propagates down the driven section in the form of the shock wave. The diaphragms were manufactured from a single-layer acetate sheet (Mylar) of 0.125 mm, which ruptured at a mean pressure of 90 ± 2 kPa.

To record the incident and reflected pressure profiles, two Kistler 603B 0–200 bar piezo-electric pressure sensors are instrumented in the shock tube. An incident pressure sensor was mounted inside the shock tube at 1100 mm from the end of the shock tube, while the reflected pressure sensor was mounted on a portable stand used to hold the sample at a central location within the shock tube Figure 3. The testing arrangement was set up to simulate a blast wave interacting with a wall with and without auxetic structure protection.

Data was acquired using a General purpose Imatek® C3008 Data Acquisition System coupled with a Kistler® 5017B microprocessor-controlled multichannel charge amplifier, at a rate of 3 MHz over a time duration of 100 ms. To ensure event capture a pre-trigger of 30 ms was used, which was initiated using a physical disk gauge located offset but in line with the incident pressure gauge. DPlot (v.2.3.5.7) was used for creating pressure-time graphs which were analysed to determine peak transmitted pressure and positive phase impulse (i_s) recorded during each shock tube test. Positive phase impulse was measured through the integration of pressure-time curves.

Results

Static compression testing

Figure 4 details the compressive stress-strain responses of each honeycomb structure, with deformation behaviour provided in Supplemental Information A. The response profile of +ve 30°

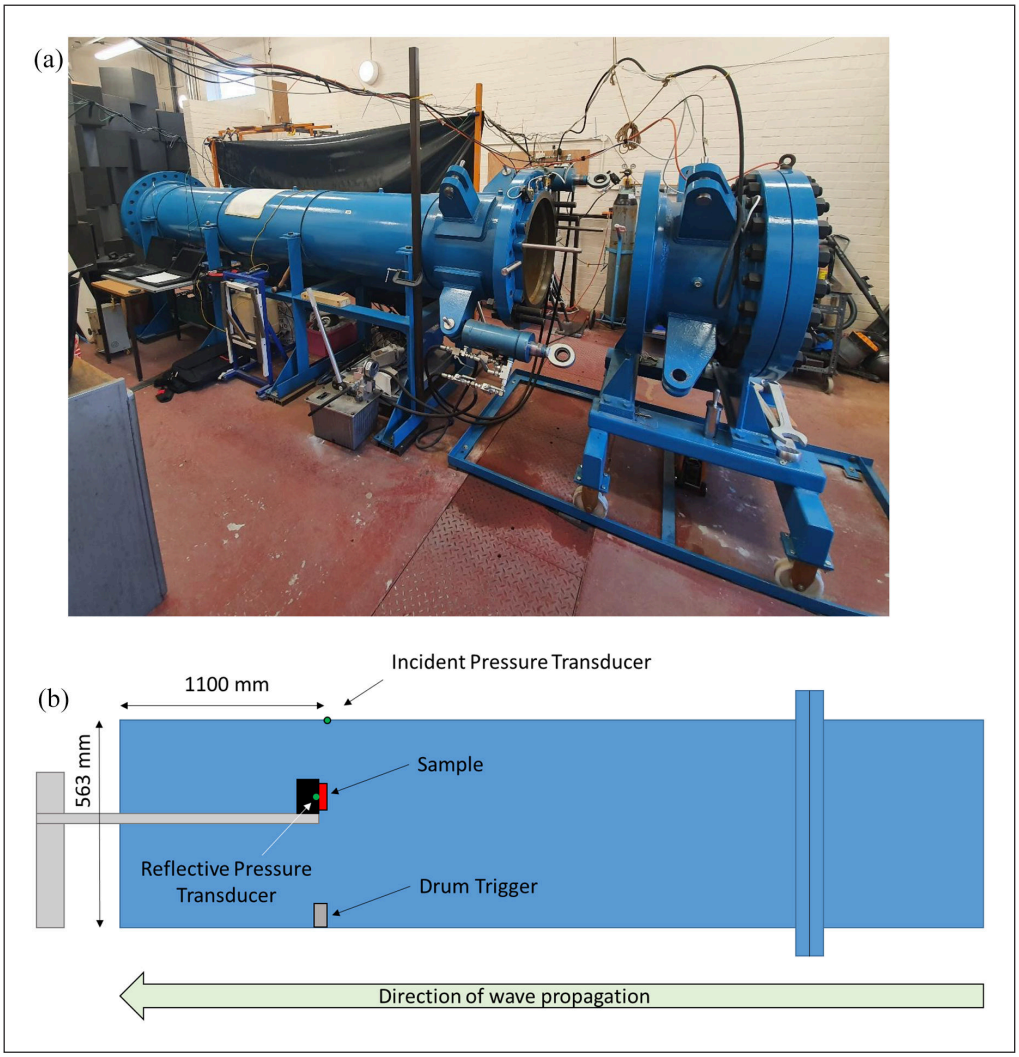


Figure 3. (a) Cranfield University Shock tube in an open position and (b) diagram of experimental setup (not to scale).
Blue section represents the shock tube.

honeycomb structure shows a linear elastic phase deformation until densification is achieved, with no distinct plateau region evident.

The +ve 15° honeycomb structure exhibited a similar response to +ve 30° but with a more defined plateau region. No district yield point was evident, instead a steady levelling of the profile akin to the plateau region was observed between 0.1 and 0.45 strain which then transitions to a densification behaviour. The difference in behaviour between the salient geometries is suspected to be caused by how the honeycomb structures deform. For the +ve 30° samples, deformation first begins about the central most cell. As loading continues, the central cell continues to flatten, resulting in the surrounding cells deforming while the outer most cells mostly retain their structure. Eventually densification occurs centrally while outer samples retain some semblance of original

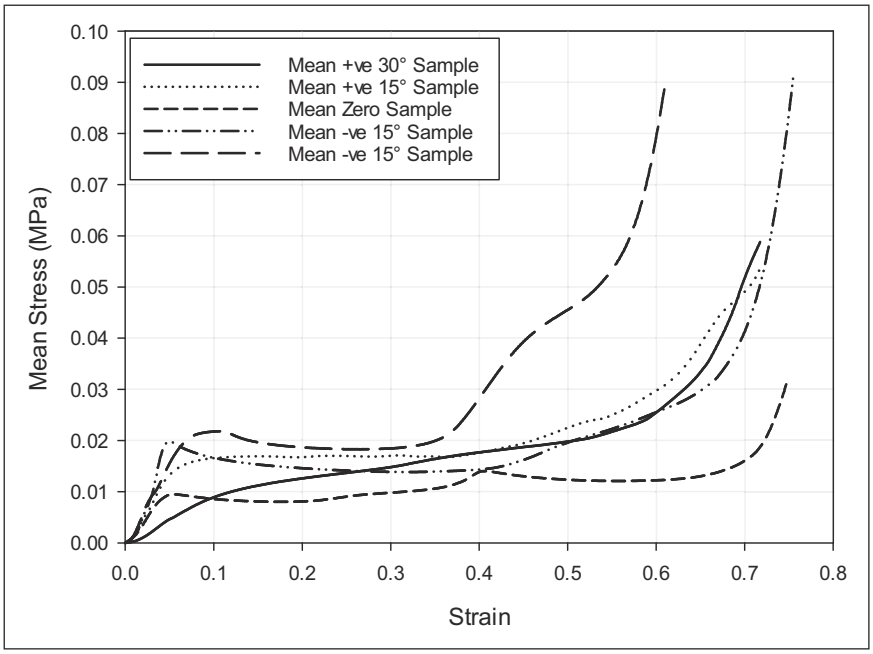


Figure 4. Mean stress-strain response of 3D printed pliable honeycomb samples (all geometries) acquired through the static compression test.

structure, until full densification occurs. During this process, there is a comparable deformation across all cells about the central axis. Alternatively, for the +ve 15° salient geometries, while initial deformation occurs about the central cell, further deformation causes the surrounding cells to deform non-uniformly resulting in cells being elongated, compressed and rotated, until densification occurs. It is interesting to note that at the completion of the test at 0.7 strain, the +ve 30° samples still retain some non-fully deformed cells.

A similar response was observed for both re-entrant structures, which is comparable to those reported in the literature (Chan and Evans, 1997a). In both traces, a linear elastic region followed by non-linear elastic phase (plateau region), indicating buckling of cell walls, can be observed prior to densification. When compared to the –ve 30°, the –ve 15° re-entrant structure exhibited a slightly lower yield limit but had a greater plateau region which in turn can be attributed to a greater energy absorption.

Overall, the Zero honeycomb exhibited the lowest strength but the greatest strain to densification. Observational analysis found that unlike the other sample geometries, the Zero geometry cells exhibited cell collapse in two stages. First the top two cell rows sheared, with minimal deformation of the lower rows. As compression continued to occur these top two rows continued to shear until full densification has occurred and returning the lower cells to their original position be it with some evidence of deformation about the top of the cells connected to those in row two. Once the top two layers are fully densified, the bottom two cell rows repeat the same behaviour exhibited in the top two cell layers. The initiation of this second densification can be seen in Figure 4 where a small peak occurs at approximately 0.4 strain. Once this second phase of densification has occurred the sample then experiences the onset of full densification around 0.7 strain. Following post

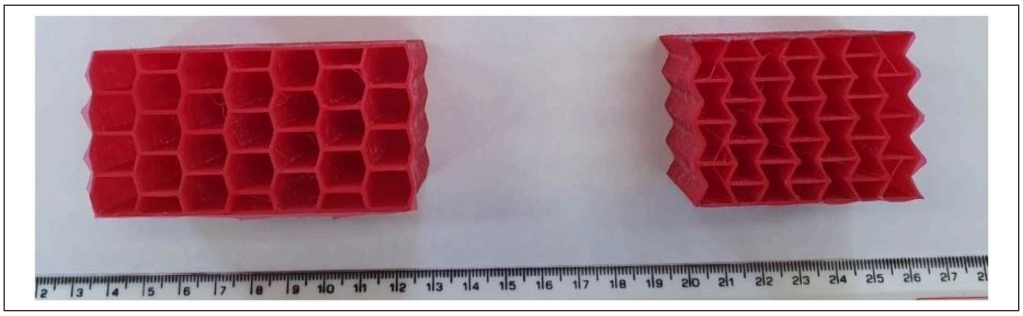


Figure 5. Example of salient honeycomb and re-entrant of shock tube samples post experiment.

compression of a sample, after a limited time period of a few minutes, samples are shown to return to their original structure indicating elastic buckling of the vertical strut members.

In summary, the repeatability of 3D printed honeycomb structures was demonstrated via quasi-static compression testing with the mean values given in Figure 4. As expected, a comparable/repeatable performance was observed. The profile traces in all samples showed a linear elastic phase, followed by non-linear elasticity region and plateau region prior to densification. Additionally, two −ve 30° samples were re-tested after 7 days and indicated comparable behaviour. It is pertinent to highlight that such a response is very difficult to attain from the conventional foam. This indicates the repeatability of 3D printing technique for the development of any cellular honeycomb structure.

Shock tube testing

Optical images were captured post experiment to ascertain if there was any discernible damage to structures (see Figure 5); no noticeable damage was observed.

Shock tube experiments demonstrated a consistent response throughout the range of 24 tests, where the average of incident channel pressure, recorded by ImpAcqt analysis software, was 38.43 ± 2.6 kPa. The duration of the positive phase was found repeatable with the average value of 5.4 ± 0.14 ms, and the mean impulse value for the positive phase was 0.093 ± 0.0017 kPa-sec.

The pressure profile of the shock tube experiments was mostly similar to the Friedlander curve (Tasissa et al., 2016) for ideal blast wave, comprising of a sudden increase of pressure from ambient to peak overpressure in the positive phase, exponential decay in pressure to the negative phase and finally settling of the trace to the ambient pressure (Cormie et al., 2009). The major deviation from the idealised Friedlander curve was the presence of an extended negative pressure phase, which often fails to return to ambient, but shares many of the peak characteristics of the incident pressure profile. The reason for this is currently unclear, especially as post-inspection of the sensor indicated no noticeable displacement of the transmitted pressure gauge, however literature suggest any deviation in shape may indicate changes in behaviour such as disruption to the jig or transducer movement (Bloodworth-Race et al., 2021).

A consistent pressure-time history of transmitted pressure and incident pressure is shown in Figure 6. The time interval of the incident and transmitted pressure was comparable with slight deviations noticeable between experiments, which are consistent within the error expected with shock tube testing. The impulse response of the positive phase was observed to be comparable between structures.

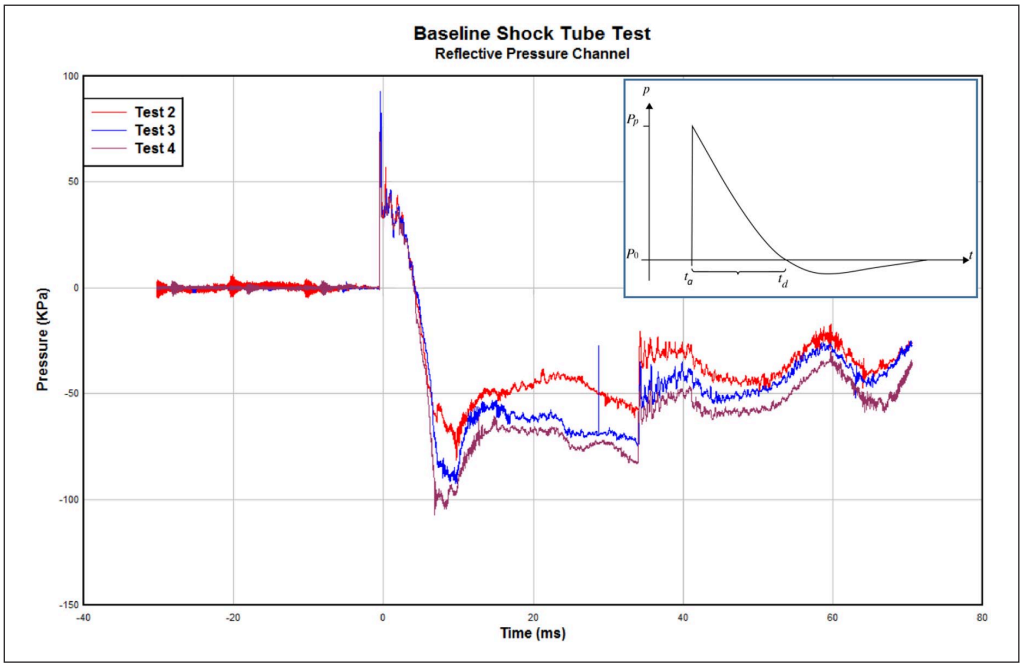


Figure 6. Raw Pressure-time measurements of baseline data where the sample response is similar in the positive phase. Test 1 omitted due to translation in the Y-axis due to sensor movement. Example of Friedlander curve provided for reference of typical behaviour.

Figure 7 shows the mean transmitted pressure and impulse time profiles for each design tested, while Table 3 details the mean transmitted maximum peak pressure and impulse values for each tested design. The response of 0° cell structure was comparable to the baseline, where a mean maximum peak transmitted pressure of 2.7 kPa higher than the baseline average was recorded. Considerable amplification of the transmitted pressure was observed in the pressure-time profiles of both the +ve 15° and +ve 30° structures, with amplification between two to three times higher noted. The results show that both the positive structures (+ve 15° and +ve 30° honeycomb) exhibited highly varied responses in transmitted pressure. From the data it is evident that once the cell structure internal angle decreases to 0° or less, the results are not as varied (approximately 10% standard deviation for all other structures). Negative structures displayed a transmitted pressure lower than the baseline indicating the mitigation of the blast loading. The –ve 15° exhibited a lower mean value than their –ve 30° counterparts, due to the standard deviation between reported values, there is likely to be some overlap in mitigation behaviour.

Discussion

Quantitative analysis of all geometries demonstrated that the positive angled structure showed consistent blast amplification response. Upon increasing the salient angle of the structural cells the mean transmitted peak transmitted pressure increases from two times the baseline value to three times; however, the impulse remains comparable to the baseline value. It can be postulated that in the salient structured cells (+ve 15° and +ve 30°), when the blast loading is applied, the physical structure is unable to mechanically resist the loading during the traditional plateau phase (seen in

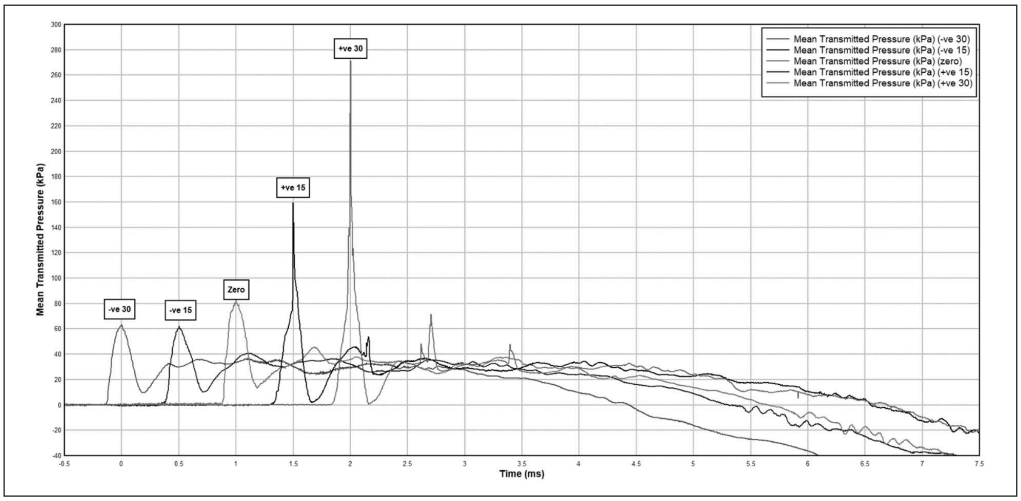


Figure 7. Mean transmitted Pressure-Time profiles for each design tested. Profiles have been offset from each other by 0.5 ms to aid readership. Full colour version normalised about 0 ms is available in Supplemental Information B.

Table 3. Mean transmitted maximum peak pressure and impulse values for each design tested.

Sample	Mean transmitted maximum peak pressure (kPa)	Mean impulse (kPa-sec)
Baseline (no Sample)	80.29 ± 8.74	0.14 ± 0.01
−ve 30° re-entrant	70.92 ± 8.57	0.13 ± 0.01
−ve 15° re-entrant	61.96 ± 6.06	0.13 ± 0
0° cell	83.00 ± 4.54	0.13 ± 0.01
+ve 15° salient honeycomb	159.49 ± 88.84	0.14 ± 0.01
+ve 30 salient honeycomb	272.01 ± 91.57	0.13 ± 0.02

Mean values calculated by taking the maximum transmitted peak pressure value from each experiment and averaged about the number of tests per geometry (see Table 1).

porous materials), and results in premature cell collapse, leading to early onset of densification. This is supported by the results in Figure 6, where both salient structures fail to exhibit the stress-strain behaviour synonymous with traditional non-auxetic porous structures under quasi-static loading. As blast loading is a high strain rate event, the open cell nature of this structure means that fluid filled pores are expelled under blast loading. As deformation occurs, there is a work done component against the viscosity and subsequent friction of the fluid. It is acknowledged that while work done against the viscosity of the fluid is strain-rate dependent (Gibson and Ashby, 1988; Jobling, 1991), due to the fixed loading conditions used herein, the influence of this behaviour cannot be characterised under these experimental conditions and therefore considered an experimental constant. However, it is recognised that the complex geometries employed within this study are likely to influence the viscosity work done.

The geometries utilising the re-entrant angled structures, demonstrated a better blast mitigation response, with values up 23% lower than the baseline. While the –ve 15° structures exhibited the greatest mitigation behaviour, it is unknown if this is the optimum angle for blast loading generally

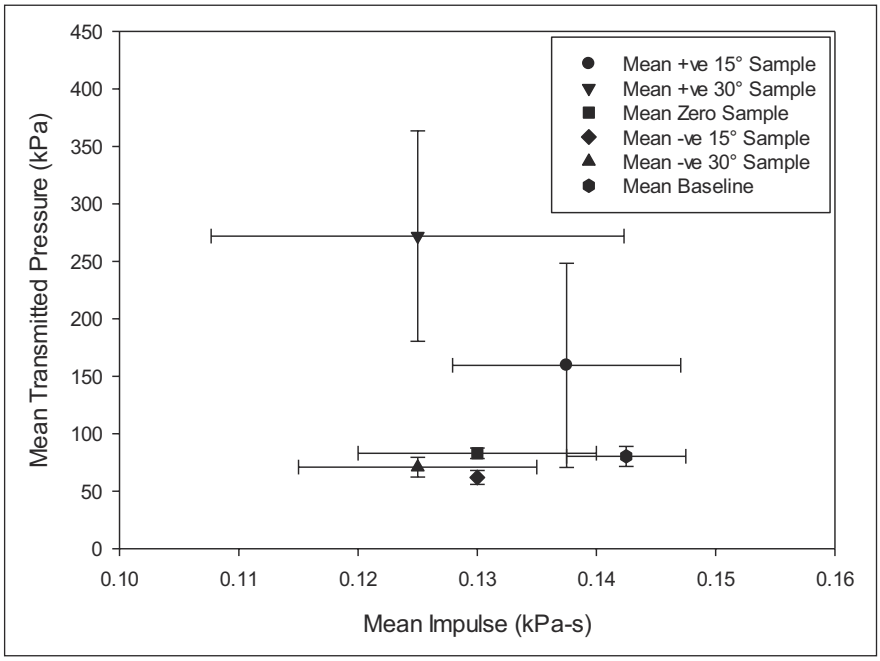


Figure 8. Mean peak transmitted pressure versus impulse response of tested structures with error provided by standard deviation.

(or just this research), as the work presented uses a fixed loading profile. This is something that requires future investigation as the negative Poisson's ratio of the re-entrant honeycomb the structure under blast compression will naturally contract. This contraction will inevitably influence the time taken to reach densification and thus in a high intensity blast loading event could cause increased damage of the re-entrant honeycomb structure. This observation will need to be considered and investigated further via higher blast loading experiments. The value of the optimum angle could change under different loading regimes, requiring further studies. As with 3D printing there are many parameters to be defined to achieve optimal material behaviour.

It was observed during testing that when the salient angled samples were compressed under constant load, there was minimal physical resistance as they propagate perpendicular to the load. Conversely, for the re-entrant angled structures, it is found that the cells interact independent of the distance between the struts, but instead some initial auxetic behaviour occurs about the central row, which results in deformation occurring at the sample corners. As compressive loading continues to be applied, cells start to shear and deform from RHS to LHS. During this phase of deformation, the samples begin to take on an arrow like shape. As loading continues to be applied, continued cell deformation occurs, causing the cells to transition from re-entrant shape to more of a '*Z*' geometry. As loading continues, two distinct areas of densification start to form, above and below the central cell rows and form as parts of the new *Z* geometries start to interact and compress on to each other. By increasing the local resistance to the load, a greater loading force is required to overcome the increase in local density/energy absorption of the structure. As testing continues this behaviour spreads to other cells until whole rows of cells are compressed and resulting in full densification. See Supplemental Information A for detailed observations for each step of this behaviour per sample type.

From Figure 8, if we examine the impulse response in isolation, all structures demonstrated some blast mitigation when considering the mean response, albeit for positive +ve 15°, +ve 30°

and zero the standard deviation overlaps the baseline, and therefore highlights the need for further testing to confirm the mitigation behaviour of these structures. Alternatively, both re-entrant structures (irrespective of cell angle) exhibited consistent impulse mitigation (when compared to the baseline), with the –ve 15° being the more repeatable. Therefore, it can be stated that the presence of a negative cell angle is a factor in reducing the overall impulse.

The re-entrant structures demonstrate a drastic reduction in peak transmitted pressure when compared to the salient counterparts. Interestingly, both the re-entrant and zero cell structures demonstrate a high level of repeatability, while the salient structures show a less consistent response, highlighting that the presence of a salient cell structure elucidates a more variable response. This indicates that 0° represents a natural repeatable threshold at which point the structures will effectively mitigate the blast loading. Therefore, the data presented here suggests that the re-entrant structures represent a novel, viable solution to blast mitigation. However the authors acknowledge that the exact mechanisms for this are not yet fully explained, and are subject to ongoing research in this field, however research suggests material concentration and bulging of the auxetic core are key parameters in the re-entrants response to blast (Qi et al., 2017). Furthermore, it remains unclear why both honeycombs exhibit much higher peak transmitted pressures than those with lower compressive strengths. Except for the zero geometry samples, all geometries comprised of struts of equal lengths and thicknesses, suggestion the geometry itself plays a role.

The research was further extended due to the variation in the sample surface area. The surface area in this study is defined as the flat face of the sample, presented to the blastwave. Due to the fixed number of cells within each structure type (as detailed in materials and methods) the surface area varies between specimens and as such needs to be normalised to enable true comparison. It was not appropriate to reduce samples down to the same volumetric measurements as this would comprise the fixed cellular structure which is the focus of this study. The results from normalisation are presented in Figure 9.

After normalisation, the salient structures continue to demonstrate the best reduction of impulse while the re-entrant structures are better at pressure reduction. However, in response of structures to blast, damage response is often quantified using pressure-impulse charts. Since both properties are important when trying to reduce damage, from the work presented herein, both salient and re-entrant structures mitigate impulse, however only re-entrant structures offer a reduction in peak transmitted pressure.

The data was additionally normalised about relative density (Figure 10) due to its influence on energy absorption in sacrificial cladding applications. Overall, samples can be shown to cluster based about its relative density, with the highest relative density exhibiting the lowest normalised transmitted pressure and impulse. As relative density reduced, typically the normalised transmitted pressure and impulse increased. Interestingly, re-entrant −ve 15° was an outlier to this behaviour, as it was seen that although it had a relative density less than −ve 30° and zero, its normalised transmitted pressure was comparable even though its impulse was greater. Relative density however is unlikely to be the only factor that determines performance, as the saliant honeycombs +ve 15° and +ve 30° of comparable relative densities exhibited different normalised impulses and transmitted pressures. This suggests that either the honeycomb geometry or surface area (both experimentally variable within this study) are also factors in influencing performance, however to a lesser extent than the relative density. While the degree of influence these additional parameters have is currently unknown.

Conclusions

A series of honeycomb structure samples were prepared through 3D printing by varying the cell angles between salient and re-entrant (–ve 30° to +ve 30°). Blast mitigation response was

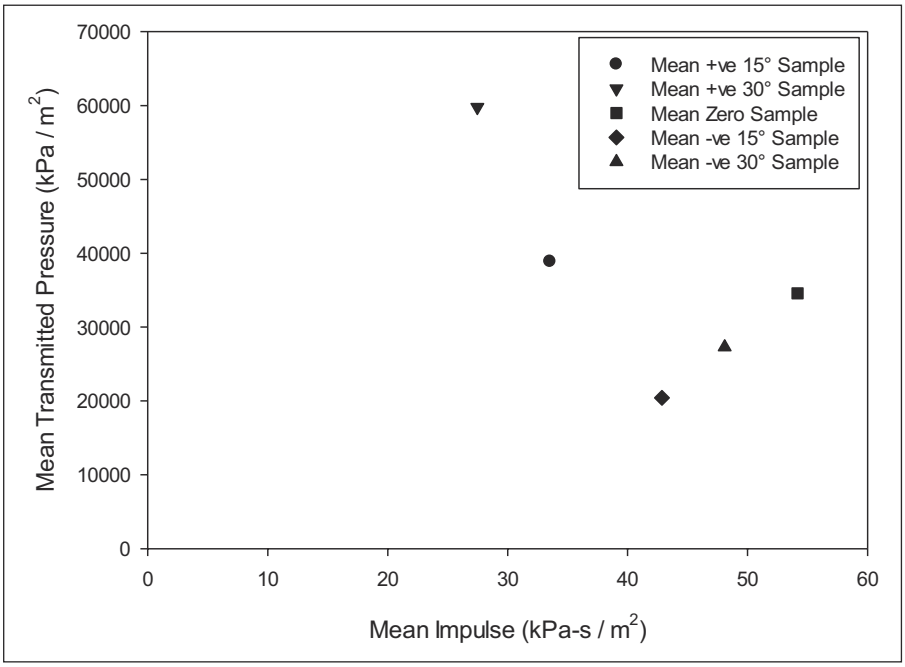


Figure 9. Mean peak transmitted pressure versus impulse response of tested structures normalised about surface area.

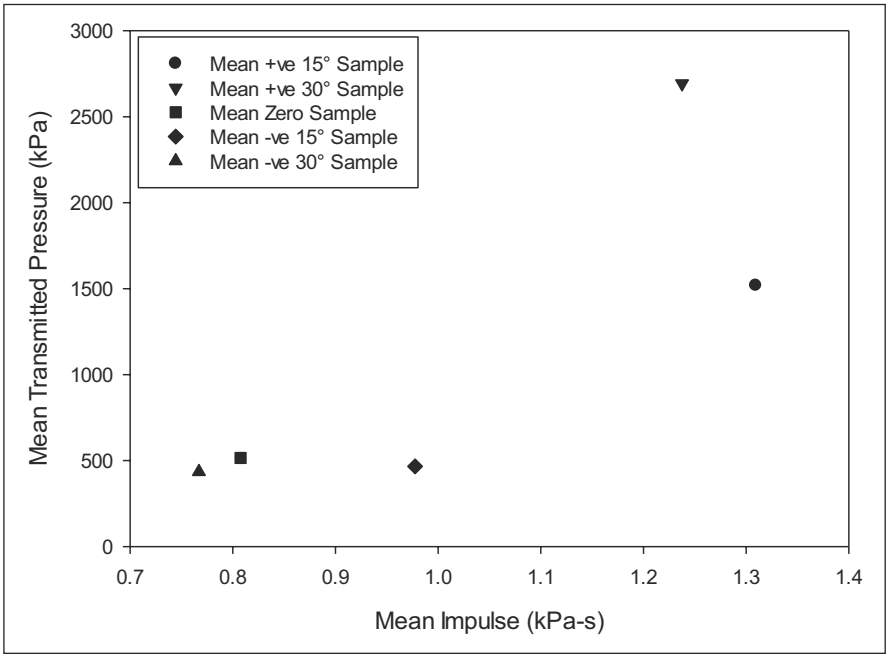


Figure 10. Mean peak transmitted pressure versus impulse response of tested structures normalised about relative density.

quantified by a constant loading profile delivered via shock tube. Samples were analysed quasi-static compressive testing and pressure-impulse response.

1. 3D printing is a suitable method for the manufacturing of auxetic foam structures for consistency and repeatability in contrast with the conventional fabrication method.
2. Static-compression results of negative angled structures demonstrated a comparable response to literature. The response profile of –ve 15° auxetic foam structures exhibited the greatest energy absorption.
3. The response demonstrated by –ve 15° auxetic foam samples (with 23% blast mitigation) was observed to be better than –ve 30° auxetic re-entrant honeycomb structures, with 12% mitigation response. Critical angle yet to be identified.
4. Blast amplification response was shown by positive angled auxetic re-entrant honeycomb structures, with an extensively higher peak transmitted pressure by +ve 30° salient foam samples (277% blast amplification) as compared to +ve 15° salient foam samples (60% blast amplification).

As both impulse and pressure are important when trying to reduce blast damage to structures, both salient and re-entrant structures mitigate impulse, however only re-entrant structures offer a reduction in peak transmitted pressure, requiring further research. Future studies should aim to expanded upon the results herein using more traditional materials and larger explosive charge sizes, along with the relationship between honeycomb geometry parameters and relative density. Additional auxetic cellular geometries such as arrowhead, chiral and star should also be investigated due to their better performance as indicated in literature and will be used as benchmarks for future designs.

Declaration of conflicting interests

The author(s) declared no potential conflicts of interest with respect to the research, authorship, and/or publication of this article.

Funding

The author(s) disclosed receipt of the following financial support for the research, authorship, and/or publication of this article: This work was funded by Cranfield University

ORCID iD

Richard Critchley https://orcid.org/0000-0001-5423-9859

Supplemental material

Supplemental material for this article is available online.

Note

1. Due to the hydroscopic nature of TPU-95A, the material was heated at 70°C for 30 min.

References

Alderson A (1999) A triumph of lateral thought. *Chemistry & Industry* 10: 384–391.

Andami H and Toopchi-Nezhad H (2020) Performance assessment of rigid polyurethane foam core sandwich panels under blast loading. *International Journal of Protective Structures* 11(1): 109–130.

Andreotti R, Colombo M, Guardone A, et al. (2015) Performance of a shock tube facility for impact response of structures. *International Journal of Non-Linear Mechanics* 72: 53–66.

Arifurrahman F, Critchley R and Horsfall I (2020) Experimental and numerical study of auxetic sandwich panels on 160 grams of PE4 blast loading. *Journal of Sandwich Structures and Materials*. Epub ahead of print 30 September 2020. DOI: 10.1177/1099636220961756.

Attard D, Farrugia PS, Gatt R, et al. (2020) Starchirals–A novel class of auxetic hierarchal structures. *International Journal of Mechanical Sciences* 179: 105631.

Aune V, Fagerholt E, Langseth M, et al. (2016) A shock tube facility to generate blast loading on structures. *International Journal of Protective Structures* 7(3): 340–366.

Bezazi A and Scarpa F (2007) Mechanical behaviour of conventional and negative Poisson's ratio thermoplastic polyurethane foams under compressive cyclic loading. *International Journal of Fatigue* 29(5): 922–930.

Bezazi A and Scarpa F (2009) Tensile fatigue of conventional and negative Poisson's ratio open cell PU foams. *International Journal of Fatigue* 31(3): 488–494.

Bloodworth-Race S, Critchley R, Hazael R, et al. (2021) Testing the blast response of foam inserts for helmets. *Heliyon* 7(5): e06990.

Chan N and Evans KE (1997a) Fabrication methods for Auxetic foams. *Journal of Materials Science* 32(22): 5945–5953.

Chan N and Evans KE (1997b) Microscopic examination of the microstructure and deformation of conventional and auxetic foams. *Journal of Materials Science* 32(21): 5725–5736.

Chan N and Evans KE (1999a) The mechanical properties of conventional and auxetic foams. Part I: Compression and tension. *Journal of Cellular Plastics* 35(2): 130–165.

Chan N and Evans KE (1999b) The mechanical properties of conventional and auxetic foams. Part II: Shear. *Journal of Cellular Plastics* 35(2): 166–183.

Chen CP and Lakes RS (1995) Analysis of the structure – property relations of foam materials. *Cellular Polymers* 14(3): 186–202.

Chen L, Xiao Y, Xiao G, et al. (2015) Test and numerical simulation of truck collision with anti-ram bollards. *International Journal of Impact Engineering* 75: 30–39.

Choi JB and Lakes RS (1991) Design of a fastener based on negative Poisson's ratio. *Cellular Polymers* 10(3): 205–212.

Choi JB and Lakes RS (1995a) Analysis of elastic modulus of conventional foams and of re-entrant foam materials with a negative Poisson's ratio. *International Journal of Mechanical Sciences* 37(1): 51–59.

Choi JB and Lakes RS (1995b) Nonlinear analysis of the Poisson's ratio of negative Poisson's ratio foams. *Journal of Composite Materials* 29(1): 113–128.

Cormie D, Mays G and Smith P (2009) *Blast Effects on Buildings*. London: Thomas Telford Publishing.

Critchley R, Corni I, Wharton JA, et al. (2013a) A review of the manufacture, mechanical properties and potential applications of auxetic foams. *Advanced Functional Materials* 250: 1963–1982.

Critchley R, Corni I, Wharton JA, et al. (2013b) The preparation of auxetic foams by three-dimensional printing and their characteristics. *Advanced Engineering Materials* 15(10): 980–985.

Dannemann KA and Lankford J (2000) High strain rate compression of closed-cell aluminium foams. *Materials Science and Engineering A* 293(1–2): 157–164.

Ding Y, Wang S, Zhao K, et al. (2016) Blast alleviation of cellular sacrificial cladding: A nonlinear plastic shock model. *International Journal of Applied Mechanics* 08(04): 1650057.

Draganić H, Gazić G and Varevac D (2019) Experimental investigation of design and retrofit methods for blast load mitigation – A state-of-the-art review. *Engineering Structures* 190: 189–209.

Dziewit P, Płatek P, Janiszewski J, et al. (2017) Mechanical response of additive manufactured regular cellular structures in quasi-static loading conditions-part I experimental Investigations. In: 7th International conference mechanics and materials in design at, Albufeira/Portugal, 11–15 June 2017.

Evans KE and Alderson A (2000) Auxetic materials: Functional materials and structures from lateral thinking! *Advanced Materials* 12(9): 617–628.

Evans KE, Nkansah MA and Hutchinson IJ (1994) Auxetic foams: Modelling negative Poisson's ratios. *Acta Metallurgica et Materialia* 42(4): 1289–1294.

Farrell DT, McGinn C and Bennett GJ (2020) Extension twist deformation response of an auxetic cylindrical structure inspired by deformed cell ligaments. *Composite Structures* 238: 111901.

Friis EA, Lakes RS and Park JB (1988) Negative Poisson's ratio polymeric and metallic foams. *Journal of Materials Science* 23(12): 4406–4414.

Gao Q, Ge C, Zhuang W, et al. (2019) Crashworthiness analysis of double-arrowed auxetic structure under axial impact loading. *Materials & Design* 161: 22–34.

Gaskell D (2011) *Forensic Investigation of Explosions*. Boca Raton, FL: CRC Press.

Gaspar N (2010) A granular material with a negative Poisson's ratio. *Mechanics of Materials* 42(7): 673–677.

Gibson LJ and Ashby MF (1988) *Cellular Solids: Structure and Properties*. London: Cambridge University Press.

Grujicic M, Galgalikar R, Snipes JS, et al. (2013) Multi-physics modeling of the fabrication and dynamic performance of all-metal auxetic-hexagonal sandwich-structures. *Materials & Design* 51: 113–130.

Guruprasad S and Mukherjee A (2000a) Layered sacrificial claddings under blast loading part I — Analytical studies. *International Journal of Impact Engineering* 24(9): 957–973.

Guruprasad S and Mukherjee A (2000b) Layered sacrificial claddings under blast loading part II — Experimental studies. *International Journal of Impact Engineering* 24(9): 975–984.

Habib FN, Iovenitti P, Masood SH, et al. (2017) In-plane energy absorption evaluation of 3D printed polymeric honeycombs. *Virtual and Physical Prototyping* 12(2): 117–131.

Habib FN, Iovenitti P, Masood SH, et al. (2018) Cell geometry effect on in-plane energy absorption of periodic honeycomb structures. *The International Journal of Advanced Manufacturing Technology* 94(5–8): 2369–2380.

Hanssen AG, Enstock L and Langseth M (2002) Close-range blast loading of aluminium foam panels. *International Journal of Impact Engineering* 27(6): 593–618.

Hanssen AG, Girard Y, Olovsson L, et al. (2006) A numerical model for bird strike of aluminium foam-based sandwich panels. *International Journal of Impact Engineering* 32(7): 1127–1144.

Hu B, Li GQ, Chen SW, et al. (2011) State-of-the-Art review on anti-ram bollards. *Applied Mechanics and Materials* 90-93: 3206–3213.

Imbalzano G, Linforth S, Ngo TD, et al. (2018) Blast resistance of auxetic and honeycomb sandwich panels: Comparisons and parametric designs. *Composite Structures* 183: 242–261.

Jiang Y and Li Y (2018) 3D printed Auxetic mechanical metamaterial with chiral cells and re-entrant cores. *Scientific Reports* 8(1): 2397.

Jin X, Wang Z, Ning J, et al. (2016) Dynamic response of sandwich structures with graded auxetic honeycomb cores under blast loading. *Composites Part B Engineering* 106: 206–217.

Jobling A (1991) An introduction to rheology H. A. Barnes, J. F. Hutton and K. Walters, Elsevier Science Publishers, Amsterdam, 1989. Pp. V + 199, price $6050/dfl 115.00. ISBN 0-444-87469-0. *Polymer International* 25(1): 61–61.

Kalubadanage D, Remennikov A, Ngo T, et al. (2020) Close-in blast resistance of large-scale auxetic re-entrant honeycomb sandwich panels. *Journal of Sandwich Structures and Materials*. Epub ahead of print 27 November 2020. DOI: 10.1177/1099636220975450.

Lakes R (1987) Foam structures with a negative Poisson's ratio. *Science* 235(4792): 1038–1040.

Lakes R (1991) Deformation mechanisms in negative Poisson's ratio materials: Structural aspects. *Journal of Materials Science* 26(9): 2287–2292.

Lakes R (1992) New materials – No contractile obligations. *Nature* 358(6389): 713–714.

Lakes RS (1993) Design considerations for materials with negative Poisson's ratios. *Journal of Mechanical Design* 115(4): 696–700.

Lakes RS and Elms K (1993) Indentability of conventional and negative Poisson's ratio foams. *Journal of Composite Materials* 27(12): 1193–1202.

Lan X, Feng S, Huang Q, et al. (2019) A comparative study of blast resistance of cylindrical sandwich panels with aluminum foam and auxetic honeycomb cores. *Aerospace Science and Technology* 87: 37–47.

Lan X-K, Huang Q, Zhou T, et al. (2020) Optimal design of a novel cylindrical sandwich panel with double arrow auxetic core under air blast loading. *Defence Technology* 16: 617–626.

Lee T and Lakes RS (1997) Anisotropic polyurethane foam with Poisson's ratio greater than 1. *Journal of Materials Science* 32(9): 2397–2401.

Lisiecki J, Kłysz S, Błażejewicz T, et al. (2014) Tomographic examination of auxetic polyurethane foam structures. *physica status solidi (b)* 251(2): 314–320.

Liu YP and Hu H (2010) A review on auxetic structures and polymeric materials. *Scientific Research and Essays* 5(10): 1052–1063.

Li X, Zhang P, Wang Z, et al. (2014) Dynamic behavior of aluminum honeycomb sandwich panels under air blast: Experiment and numerical analysis. *Composite Structures* 108: 1001–1008.

Ma GW and Ye ZQ (2007a) Analysis of foam claddings for blast alleviation. *International Journal of Impact Engineering* 34(1): 60–70.

Ma GW and Ye ZQ (2007b) Energy absorption of double-layer foam cladding for blast alleviation. *International Journal of Impact Engineering* 34(2): 329–347.

Mukai T, Kanahashi H, Miyoshi T, et al. (1999) Experimental study of energy absorption in a close-celled aluminum foam under dynamic loading. *Scripta Materialia* 40(8): 921–927.

Neuberger A, Peles S and Rittel D (2007a) Scaling the response of circular plates subjected to large and close-range spherical explosions. Part I: Air-blast loading. *International Journal of Impact Engineering* 34(5): 859–873.

Neuberger A, Peles S and Rittel D (2007b) Scaling the response of circular plates subjected to large and close-range spherical explosions. Part II: Buried charges. *International Journal of Impact Engineering* 34(5): 874–882.

Novak N, Starčevič L, Vesenjak M, et al. (2019) Blast response study of the sandwich composite panels with 3D chiral auxetic core. *Composite Structures* 210: 167–178.

Qi C, Remennikov A, Pei L-Z, et al. (2017) Impact and close-in blast response of auxetic honeycomb-cored sandwich panels: Experimental tests and numerical simulations. *Composite Structures* 180: 161–178.

Qi C, Yang S, Yang L-J, et al. (2013) Blast resistance and multi-objective optimization of aluminum foam-cored sandwich panels. *Composite Structures* 105: 45–57.

Remennikov A, Kalubadanage D, Ngo T, et al. (2019) Development and performance evaluation of large-scale auxetic protective systems for localised impulsive loads. *International Journal of Protective Structures* 10(3): 390–417.

Sadot O, Anteby I, Harush S, et al. (2005) Experimental investigation of dynamic properties of aluminum foams. *Journal of Structural Engineering* 131(8): 1226–1232.

Scarpa F, Bullough WA and Lumley P (2004) Trends in acoustic properties of iron particle seeded Auxetic polyurethane foam. *Proceedings of the Institution of Mechanical Engineers Part C – Journal of Mechanical Engineering Science* 218(2): 241–244.

Scarpa F, Pastorino P, Garelli A, et al. (2005) Auxetic compliant flexible PU foams: Static and dynamic properties. *Physica Status Solidi B-Basic Solid State Physics* 242(3): 681–694.

Scarpa F and Smith FC (2004) Passive and MR fluid-coated Auxetic PU foam – Mechanical, acoustic, and electromagnetic properties. *Journal of Intelligent Material Systems and Structures* 15(12): 973–979.

Scarpa F and Tomlin PJ (2000) On the transverse shear modulus of negative Poisson's ratio honeycomb structures. *Fatigue & Fracture of Engineering Materials & Structures* 23(8): 717–720.

Scarpa F, Yates JR, Ciffo LG, et al. (2002) Dynamic crushing of Auxetic open-cell polyurethane foam. *Proceedings of the Institution of Mechanical Engineers Part C Journal of Mechanical Engineering Science* 216(12): 1153–1156.

Shahbeyk S, Petrinic N and Vafai A (2007) Numerical modelling of dynamically loaded metal foam-filled square columns. *International Journal of Impact Engineering* 34(3): 573–586.

Shim C, Yun N, Yu R, et al. (2012) Mitigation of blast effects on protective structures by aluminum foam panels. *Metals* 2: 170–177.

Shim CS and Yun NR (2010) Evaluation of closerange blast pressure mitigation using a sacrificial member. *Journal of the Earthquake Engineering Society of Korea* 14(1): 11–23.

Shirbhate PA and Goel MD (2021) A critical review of blast wave parameters and approaches for blast load mitigation. *Archives of Computational Methods in Engineering* 28(3): 1713–1730.

Smith CW, Lehman F, Wootton RJ, et al. (1999) Strain dependent densification during indentation in Auxetic foams. *Cellular Polymers* 18(2): 79–101.

Smith PD, Whalen GP, Feng LJ, et al. (2001) Blast loading on buildings from explosions in city streets. *Proceedings of the Institution of Civil Engineers – Structures and Buildings* 146(1): 47–55.

Tasissa AF, Hautefeuille M, Fitek JH, et al. (2016) On the formation of Friedlander waves in a compressed-gas-driven shock tube. *Proceedings of The Royal Society A Mathematical Physical and Engineering Sciences* 472(2186): 20150611.

Ultimaker (2018) *Technical data sheet TPU 95A*. Available at: https://www.matterhackers.com/r/0HMNp5 (accessed 6 October 2021).

Wang Y, Zhao W, Zhou G, et al. (2018) Analysis and parametric optimization of a novel sandwich panel with Double-V auxetic structure core under air blast loading. *International Journal of Mechanical Sciences* 142–143: 245–254.

Xue Z and Hutchinson JW (2004) A comparative study of impulse-resistant metal sandwich plates. *International Journal of Impact Engineering* 30(10): 1283–1305.



https://dspace.org/

Blast mitigation using polymeric 3D printed auxetic lattice structures - a preliminary study

Critchley, Richard; Hazael, Rachael; Bhatti, Kamran; Wood, David C.; Peare, Alan ...

2022-09
Sage
https://doi.org/10.1177/20414196211052062
Critchley R, Hazael R, Bhatti K, et al., (2022) Blast mitigation using polymeric 3D printed auxetic lattice structures - a preliminary study. International Journal of Protective Structures, Volume 13, Issue 3, September 2022, pp. 469-486

Downloaded from a DSpace repository. https://dspace.org/